Mechanical Technology and Engineering Insights

www.mtei.reapress.com

Mech. Technol. Eng. Insights . Vol. 2, No. 3 (2025) 210–221.

Paper Type: Original Article

Mixed Convection Heat Transfer of a Non-Newtonian Power-Law Fluid over a Vertical Wavy Surface with Internal Heat Generation or Absorption

Eisa Abdolmaleki[1,*], Hashem Saberi Najafi[2]

[1] Department of Mathematics, Tonekabon Branch, Islamic Azad University, Tonekabon, Iran; eabdolmaleki@aihe.ac.ir.
[2] Department of Applied Mathematics, Lahijan Branch, Islamic Azad University, Lahijan, Iran; hnajafi@guilan.ac.ir.

Citation:

Received: 12 October 2024 *Revised: 17 December 2024* *Accepted: 22 February 2025*	Abdolmaleki, E., & Hashem Saberi Najafi, H. (2025). Mixed convection heat transfer of a non-Newtonian power-law fluid over a vertical wavy surface with internal heat generation or absorption. *Mechanical Technology and Engineering Insights, 2*(3), 210-221.

Abstract

In the present study, combined convection heat transfer in the boundary layer flow of a non-Newtonian fluid with internal heat generation or absorption over a vertical wavy surface is investigated. A coordinate transformation is employed to convert the governing equations from the wavy geometry to an equivalent flat surface. The transformed boundary layer equations are solved numerically using the finite difference method. The effects of key parameters, including the heat generation/absorption parameter, wave amplitude, generalized Prandtl number, and power-law viscosity index, are examined through variations of the local and average Nusselt numbers as well as the skin friction coefficient. The results indicate that increasing the heat generation parameter leads to fluid heating and a corresponding reduction in the heat transfer rate in non-Newtonian fluids.

Keywords: Combined convection heat transfer, Non-Newtonian fluid, Heat generation absorption, Wavy surface.

1 | Introduction

In recent years, non-Newtonian fluids have found widespread applications in various industrial processes, particularly in thermal and cooling systems, such as polymer processing, plastic melting, and the enhancement and optimization of heat exchanger performance. Understanding heat transfer characteristics in such fluids is therefore of significant importance. Most previous investigations on non-Newtonian fluids have been conducted over smooth surfaces. However, heat transfer over wavy surfaces is of greater practical relevance due to the surface irregularities commonly encountered in engineering applications such as solar collectors,

Corresponding Author: eabdolmaleki@aihe.ac.ir
https://doi.org/10.48313/mtei.v2i3.55

condensers, and industrial heat exchangers. Consequently, the present study focuses on heat transfer over wavy surfaces. The earliest investigations in this field were carried out by Kim [1], who studied natural convection heat transfer over vertical wavy surfaces in non-Newtonian fluids. He reported that increasing the non-Newtonian power-law index reduces the boundary layer thickness. Moreover, the heat transfer coefficient increases for dilatant fluids while it decreases for pseudoplastic fluids.

Yang and Chen [2] examined natural convection heat transfer of non-Newtonian fluids over wavy surfaces in the presence of a magnetic field. Using a cubic spline method to solve the transformed equations, they showed that the temperature gradient in dilatant fluids is higher than that in pseudoplastic fluids. They also observed that increasing the magnetohydrodynamic parameter increases fluid temperature while reducing the velocity.

Wang and Chen [3] investigated combined convection boundary layer flow with magnetohydrodynamic effects over wavy surfaces with various inclination angles. They demonstrated the existence of two harmonics in the Nusselt number and skin friction distributions, where the first harmonic arises from pressure gradients and the second from diffusion and centrifugal forces. Furthermore, they studied combined convection heat transfer of non-Newtonian fluids over wavy surfaces [4], revealing that the thermal behavior near the leading edge differs from that in the downstream region.

Jang and Yan [5] analyzed combined heat and mass transfer over a wavy surface, while Molla and Hossain [6] studied the combined effects of radiation and mixed convection over a wavy surface. Hady et al. [7] investigated magnetohydrodynamic natural convection with heat generation or absorption, and Tashtoush and Al-Odat [8] explored MHD effects over compound wavy surfaces.

Elgazery and Abd Elazem [9] numerically studied unsteady MHD natural convection heat and mass transfer over a vertical wavy surface with temperature-dependent viscosity and thermal conductivity, reporting that variations in fluid properties and magnetic field strength significantly affect the velocity, temperature, and concentration fields, as well as the local skin-friction, Nusselt, and Sherwood numbers.

Parveen and Alim [10] numerically investigated MHD natural convection of a viscous incompressible fluid along a uniformly heated vertical wavy surface with temperature-dependent viscosity, using a Keller–box scheme, and demonstrated that variations in viscosity and magnetic field strength significantly influence the velocity and thermal boundary layers, leading to notable changes in the local skin-friction coefficient and Nusselt number.

Nath and Parveen [11] numerically studied MHD natural convection along a vertical wavy surface considering viscous dissipation and internal heat generation, and reported that the viscous dissipation, heat generation, and magnetic field parameters significantly affect the velocity and temperature distributions, leading to marked variations in the local skin-friction coefficient and Nusselt number.

Islam and Parveen [12] analyzed MHD natural convection along a uniformly heated vertical wavy surface considering viscous dissipation and Joule heating, and showed that the Eckert number, Joule heating, and magnetic field parameters significantly modify the velocity and temperature fields, resulting in notable variations in the local skin-friction coefficient and Nusselt number.

Amin [13] numerically investigated steady MHD natural convection along a uniformly heated vertical wavy surface, including Joule heating, internal heat generation, and viscous dissipation, using the Keller–box method, and demonstrated that these thermal and magnetic effects, as well as surface waviness, strongly influence the velocity and temperature fields, resulting in significant variations in the local skin-friction coefficient and Nusselt number.

Mirzaei Nejad et al. [14] numerically investigated MHD mixed convection of electrically conducting power-law fluids over an isothermal vertical wavy plate and showed that the applied magnetic field suppresses the velocity field, leading to a reduction in both the Nusselt number and skin-friction coefficient, with more pronounced effects for pseudoplastic fluids $(n<1)(n<1)(n<1)$, while the wavy geometry significantly alters the local heat transfer characteristics.

Heat generation or absorption in fluid flow is an important phenomenon, particularly in chemical reactions, nuclear reactors, and electronic devices. Internal heat generation alters the temperature distribution within the fluid, affecting heat transfer characteristics. Following the work of Vajravelu and Hadjinicolaou [15], the volumetric heat generation term is modeled as

$$q''' = \begin{cases} Q_0 (T - T_\infty) & T > T_\infty \\ 0 & T < T_\infty \end{cases}, \tag{1}$$

where Q_0 represents the heat generation or absorption coefficient. This formulation accounts for cases where the internal fluid temperature deviates from the ambient temperature.

In this study, combined convection boundary layer flow of a non-Newtonian fluid with internal heat generation or absorption over a sinusoidal vertical wavy surface is analyzed. A coordinate transformation is employed to map the wavy surface onto a flat one, and the transformed governing equations are solved numerically using the finite difference method. The effects of the heat generation/absorption parameter, wave amplitude, power-law index, Richardson number, and generalized Prandtl number on the Nusselt number and skin friction coefficient are investigated. Comparisons with Newtonian fluid results are also presented.

2 | Mathematical Formulation

The steady boundary layer flow of a non-Newtonian fluid over a semi-infinite vertical wavy surface is considered. The geometry of the vertical wavy surface is described by

$$\bar{S}(\bar{x}) = \bar{a} \sin^2 (\pi \bar{x}/L), \tag{2}$$

where a denotes the wave amplitude, L is the wavelength. The wavy surface is maintained at a constant temperature T_w , which is higher than the ambient fluid temperature T_∞. The free-stream velocity and the inlet velocity at the leading edge are assumed to be uniform and equal to U_∞.

Fig. 1 illustrates the physical model and the coordinate system. The x-axis is taken along the wavy surface in the direction of the flow, while the y-axis is normal to the surface.

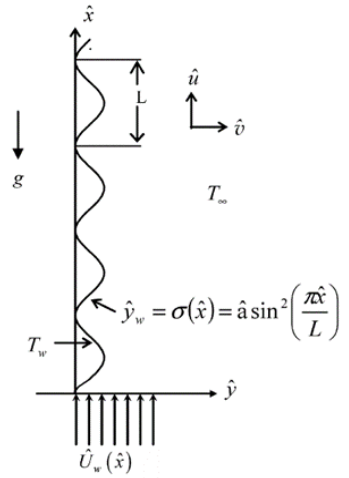

Fig. 1. Physical model and the coordinate system.

The flow is assumed to be laminar, incompressible, steady, and two-dimensional. Viscous dissipation effects are neglected. The Boussinesq approximation is employed in the momentum equation to account for buoyancy effects. Under these assumptions, the governing equations for mixed convection heat transfer of a non-Newtonian fluid with internal heat generation or absorption are written as follows:

$$\frac{\partial \bar{u}}{\partial \bar{x}}+\frac{\partial \bar{v}}{\partial \bar{y}}=0. \tag{3}$$

$$\rho\left(\bar{u}\frac{\partial \bar{u}}{\partial \bar{x}}+\bar{v}\frac{\partial \bar{u}}{\partial \bar{y}}\right)=-\frac{\partial \bar{p}}{\partial \bar{x}}+\left(\frac{\partial \tau_{\bar{x}\bar{x}}}{\partial \bar{x}}+\frac{\partial \tau_{\bar{x}\bar{y}}}{\partial \bar{y}}\right)+\rho g\beta\left(T-T_{\infty}\right). \tag{4}$$

$$\rho\left(\bar{u}\frac{\partial \bar{v}}{\partial \bar{x}}+\bar{v}\frac{\partial \bar{v}}{\partial \bar{y}}\right)=-\frac{\partial \bar{p}}{\partial \bar{y}}+\left(\frac{\partial \tau_{\bar{y}\bar{x}}}{\partial x}+\frac{\partial \tau_{\bar{y}\bar{y}}}{\partial \bar{y}}\right). \tag{5}$$

$$\rho C_p\left(\bar{u}\frac{\partial T}{\partial \bar{x}}+\bar{v}\frac{\partial T}{\partial \bar{y}}\right)=K_f\left(\frac{\partial^2 T}{\partial \bar{x}^2}+\frac{\partial^2 T}{\partial \bar{y}^2}\right)+Q_0\left(T-T_{\infty}\right). \tag{6}$$

The boundary conditions are:

I. On the wavy surface u=v=0, T=T_w.

II. In the free stream u→U_∞, T→T_∞ at y→∞.

In the above equations, $\bar{u}$ and $\bar{v}$ are the velocity components in the x and y directions, respectively; ϱ is the fluid density; p is the pressure; Cp and_P is the specific heat at constant pressure; K and n are the consistency and power-law indices, respectively; β is the thermal expansion coefficient; and Q_0 denotes the heat generation or absorption coefficient.

2.1|Coordinate Transformation and Non-Dimensionalization

To simplify the numerical treatment of the wavy surface, the Prandtl-type coordinate transformation proposed by Yao [16] is employed to map the wavy surface onto an equivalent flat surface. The non-dimensional variables are defined as:

$$\hat{x}=\frac{\bar{x}}{L},\ \hat{y}=\frac{\bar{y}-\bar{S}}{L}Re^{1/(n+1)},\ \alpha=\frac{\bar{a}}{L},\ S=\frac{\bar{S}}{L},\hat{u}=\frac{\bar{u}}{U_{\infty}}$$

$$U_w=\frac{\bar{u}_w}{U_{\infty}},\hat{v}=\frac{\bar{v}-\bar{S}'\bar{u}}{u_{\infty}}Re^{1/(n+1)},\hat{p}=\frac{\bar{p}}{\rho U_{\infty}{}^2}$$

$$\theta=\frac{T-T_{\infty}}{T_w-T_{\infty}},\ Ri=\frac{Gr}{Re^2},Re=\frac{\rho U_{\infty}^{2-n}L^n}{K},\ Q=\frac{Q_0 L}{\rho C_p U_{\infty}}$$

$$Pr=\frac{C_p K^{2/(n+1)}}{K_f}\left(\frac{\rho U_{\infty}{}^3}{L}\right)^{(n-1)/(n+1)},\ Gr=\frac{g\beta\left(T_w-T_{\infty}\right)\rho^2 L^{1+2n}U_{\infty}{}^{2(1-n)}}{K^2}.$$

Substituting the non-dimensional variables defined in *Eq. (6)* into *Eqs. (2-5)*, the transformed governing equations become:

$$\frac{\partial \hat{u}}{\partial \hat{x}}+\frac{\partial \hat{v}}{\partial \hat{y}}=0, \tag{7}$$

$$\hat{u}\frac{\partial \hat{u}}{\partial \hat{x}}+\hat{v}\frac{\partial \hat{u}}{\partial \hat{y}}=-\frac{\partial \hat{p}}{\partial \hat{x}}+Ri\theta+Re^{1/(n+1)}S'\frac{\partial \hat{p}}{\partial \hat{y}}+\left(1+S'^2\right)^n\frac{\partial}{\partial \hat{y}}\left(\frac{\partial \hat{u}}{\partial \hat{y}}\left|\frac{\partial \hat{u}}{\partial \hat{y}}\right|^{n-1}\right), \tag{8}$$

$$S''\hat{u}^2+S'Ri\theta=S'\frac{\partial \hat{p}}{\partial \hat{x}}-Re^{1/(n+1)}\left(1+S'^2\right)\frac{\partial \hat{p}}{\partial \hat{y}}, \tag{9}$$

$$\hat{u}\frac{\partial\theta}{\partial\hat{x}}+\hat{v}\frac{\partial\theta}{\partial\hat{y}}=\frac{1}{Pr}\left(1+S'^{2}\right)\frac{\partial^{2}\theta}{\partial\hat{y}^{2}}+Q\theta, \tag{10}$$

where Ri is the Richardson number, Pr is the generalized Prandtl number.

Since *Eq. (9)* indicates that the pressure gradient in the Y-direction is of the order of $O\left(Re^{-1/(n+1)}\right)$, the pressure gradient can be obtained by solving the inviscid flow equations, yielding:

$$\frac{\partial\hat{p}}{\partial\hat{x}}=-\left(1+S'^{2}\right)U_{w}U'_{w}+S'S''U_{w}{}^{2}{}_{w}. \tag{11}$$

By eliminating the pressure gradient from *Eqs. (8)* and *(9)*, the transformed momentum equation can be written as:

$$\hat{u}\frac{\partial\hat{u}}{\partial\hat{x}}+\hat{v}\frac{\partial\hat{u}}{\partial\hat{y}}=\frac{1}{1+S'^{2}}\left(-\frac{\partial\hat{p}}{\partial\hat{x}}+Ri\theta-S'S''\hat{U}^{2}\right)+$$
$$\left(1+S'^{2}\right)^{n}\frac{\partial}{\partial\hat{y}}\left(\frac{\partial\hat{u}}{\partial\hat{y}}\left|\frac{\partial\hat{u}}{\partial\hat{y}}\right|^{n-1}\right). \tag{12}$$

2.2 | Similarity Transformation

Since the leading edge represents a singular point, the following transformations are introduced to remove the singularity [6]:

$$x=\hat{x},\ v=\hat{v}\left(\frac{2\hat{x}}{U_{w}}\right)^{1/(n+1)},\ u=\frac{\hat{u}}{U_{w}},\ y=\hat{y}\left(\frac{2\hat{x}}{U_{w}}\right)^{-1/(n+1)}. \tag{13}$$

Substituting Eq. (13) into Eqs. (7), (10), and (12), the final governing equations suitable for numerical solution are obtained as:

$$2x\frac{\partial u}{\partial x}-\frac{2}{n+1}y\left(1-x\frac{U'_{w}}{U_{w}}\right)\frac{\partial u}{\partial y}+\left(\frac{2x}{U_{w}}\right)^{(n-1)/(n+1)}\frac{\partial v}{\partial y}+2x\frac{U'_{w}}{U_{w}}=0. \tag{14}$$

$$2xu\frac{\partial u}{\partial x}+\left[\left(\frac{2x}{U_{w}}\right)^{(n-1)/(n+1)}v-\frac{2yu}{n+1}\left(1-x\frac{U'_{w}}{U_{w}}\right)\right]\frac{\partial u}{\partial y}+2x\left(u^{2}-1\right)\left(\frac{S'S''}{1+S'^{2}}+\frac{U'_{w}}{U_{w}}\right)=$$
$$\frac{2x}{U_{w}{}^{2}\left(1+S'^{2}\right)}Ri\theta+\left(1+S'^{2}\right)^{n}U_{w}{}^{n-1}\frac{\partial}{\partial y}\left(\frac{\partial u}{\partial y}\left|\frac{\partial u}{\partial y}\right|^{(n-1)}\right)+\frac{2x}{U_{w}\left(1+S'^{2}\right)}M_{n}\left(1-u\right). \tag{15}$$

$$2xu\frac{\partial\theta}{\partial x}+\left[\left(\frac{2x}{U_{w}}\right)^{(n-1)/(n+1)}v-\frac{2yu}{n+1}\left(1-x\frac{U'_{w}}{U_{w}}\right)\right]\frac{\partial\theta}{\partial y}=\frac{\left(1+S'^{2}\right)}{Pr}\left(\frac{2x}{U_{w}}\right)^{(n-1)/(n+1)}\frac{\partial^{2}\theta}{\partial y^{2}}+\left(\frac{2x}{U_{w}}\right)Q\theta. \tag{16}$$

The corresponding boundary conditions are:

$$\text{at } y=0,\ \theta=1,\ u=v=0.$$
$$\text{at } y\to\infty,\ \theta\to0,\ u\to1. \tag{16}$$

2.3 | Surface Velocity Determination

The last step is to obtain the velocity of the surface. Yao [16] and Ghosh Moulic and Yao [17] investigated the velocity of inviscid flow and obtained an expression for the stream function, which had a good result for a small amplitude of wavy surface. In the present study, to obtain a more accurate solution for a higher amplitude wavelength ratio, a streamline function ψ was introduced. The transformed coordinates have been used to solve the potential flow and to determine the surface velocity. The streamline equation and the transformed coordinate can be written as follows:

$$\frac{\partial^2\psi}{\partial\tilde{x}^2}+\frac{\partial^2\psi}{\partial\tilde{y}^2}=0. \tag{17}$$

$$x=\tilde{x}\quad \eta=\tilde{y}-\tilde{S}(\tilde{x}). \tag{18}$$

Substitution of *Eq. (17)* into *Eq. (18)* yields the transformed equations for numerical solution using the SOR method. The surface velocity is then obtained as:

$$\frac{\partial^2\psi}{\partial x^2}-S''\frac{\partial\psi}{\partial\eta}-2S'\frac{\partial^2\psi}{\partial x\partial\eta}+\left(1+S'^2\right)\frac{\partial^2\psi}{\partial\eta^2}=0. \tag{19}$$

and consequently

$$U_w=\left.\frac{\partial\psi}{\partial\eta}\right|_{\eta=0}. \tag{20}$$

2.4 | Heat Transfer and Skin Friction Parameters

Using Newton's law of cooling and Fourier's law, the local Nusselt number is defined as:

$$\left(\frac{4}{Gr_{\bar{x}}}\right)^{1/2(n+1)}Nu_{\bar{x}}=-\left(\frac{1}{Rix}\right)^{1/2(n+1)}U_w{}^{1/(n+1)}\left(1+S'^2\right)^{1/2}\left.\frac{\partial\theta}{\partial y}\right|_{y=0}. \tag{21}$$

The average Nusselt number from the leading edge to a given position X is computed as:

$$\left(\frac{4}{Gr_{\bar{x}}}\right)^{1/2(n+1)}Nu_m=-\left(\frac{1}{Rix}\right)^{1/2(n+1)}\left(\frac{2}{x^n}\right)^{1/(n+1)}\times \int_0^x\left(\frac{U_w}{2x}\right)^{1/(n+1)}\left(1+S'^2\right)\left.\frac{\partial\theta}{\partial y}\right|_{y=0}dx. \tag{22}$$

The skin friction coefficient is expressed as:

$$Ri^{-1}\left(\frac{Gr}{2(n+1)x}\right)^{1/2(n+1)}C_f=\left(\frac{n+1}{2}\right)^{-1/2(n+1)}\times \left(\frac{1}{Rix}\right)^{(2n+1)/2(n+1)}U_w{}^{n(n+2)/(n+1)}\left(1+S'^2\right)^n\left(\frac{\partial u}{\partial y}\right)^n_{y=0}. \tag{23}$$

3 | Numerical Solution Method

The dimensionless *Eqs. (13)–(15)* are solved to obtain U and θ using a fully implicit finite difference numerical method. Central difference schemes are employed for the diffusion terms and transverse heat transfer, while a backward difference scheme based on the upstream flow is used for the streamwise heat transfer. The

governing equations are treated as unsteady until the flow reaches a steady-state regime. After discretization, the resulting algebraic equations are written in the form of a tridiagonal matrix as follows:

$$A_{i,j}\Omega^{n+1}{}_{i,j-1} + B_{i,j}\Omega^{n+1}{}_{i,j} + C_{i,j}\Omega^{n+1}{}_{i,j+1} = D_{i,j}, \quad (24)$$

where the terms Ω are replaced by the corresponding expressions U and θ. *Eq. (24)* has a tridiagonal form and can be readily solved using the Thomas algorithm. The solution procedure is continued until the desired convergence criterion is achieved, which is defined as:

$$\frac{\Omega^{n+1}_{i,j} - \Omega^{n}_{i,j}}{\Omega^{n}_{max}} < 5\times10^{-5}. \quad (25)$$

4 | Results and Discussion

In the present problem, since the variations of velocity and temperature gradients are more pronounced near the wavy surface in the y direction and also near the leading edge of the plate in the X direction, a finer grid is employed in these regions.

An important issue in numerical simulations is ensuring that the number of grid points is sufficient. To obtain an adequate grid resolution, the computations are initially performed using a coarse grid, and then the number of grid points is gradually increased until further refinement has a negligible effect on the results. For the present study, grid sizes of 80×70, 150×, 200×120, and 250×150and 250×150 are used. The results for the local Nusselt number show that the difference between the 200×120and 250×150 grids is less than 2%.

To verify the numerical accuracy of the present solutions, the local Nusselt number and skin-friction coefficient for the power-law indices n=0.5 and n=1 are presented in a table for Pr=10. In all cases, an excellent agreement is observed between the present results and those reported by Wang and Chen [3], confirming the accuracy and reliability of the numerical method used in this study.

Table 1. Comparison results for $Pr_g = 10, \alpha = 0.2$, $Ri = 50$.

	$\left(4/Gr_{g\bar{x}}\right)^{1/2(n+1)} Nu_{\bar{x}}$				$Ri^{-1}\left(Gr_g/2(n+1)x\right)^{1/2(n+1)} C_f$			
	Present n=1.5	Wang and Chen [3] n=1.5	Present n=0.5	Wang and Chen [3] n=0.5	Present n=1.5	Wang and Chen [3] n=1.5	Present n=0.5	Wang and Chen [3] n=0.5
X=1	1.06475	1.07523	1.22493	1.23568	0.96418	0.95629	0.625465	0.633329
X=1.5	1.06363	1.06973	1.38154	1.40027	1.06180	1.04536	0.622462	0.635871
X=2.0	1.00626	0.99987	1.31376	1.32065	0.99479	0.98761	0.560732	0.57322
X=3.0	0.96642	0.97332	1.364818	1.37263	1.02584	1.01096	0.528773	0.53265

The effect of heat generation or absorption on the heat transfer rate is illustrated in *Fig. 2* through the variation of the local Nusselt number for Q=−0.2-0.2, and Ri=10. It is observed that the heat transfer rate from the heated surface decreases with increasing heat generation parameter. Since heat generation increases the fluid temperature near the surface (*Fig. 3*), this reduction is expected. In contrast, in the presence of heat absorption (Q<0), a layer of cooler fluid forms near the heated surface, resulting in an enhancement of the heat transfer rate.

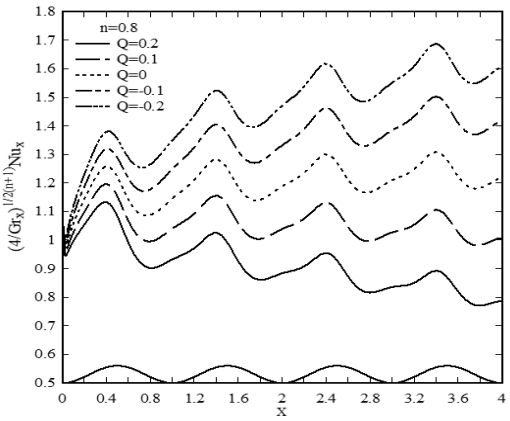

Fig. 2. Axial distribution of the local Nusselt number $\left(4/Gr_{\bar{x}}\right)^{1/2(n+1)} Nu_{\bar{x}}$ for α=0.1, Ri=10, Pr=20, n=0.8, and different Q.

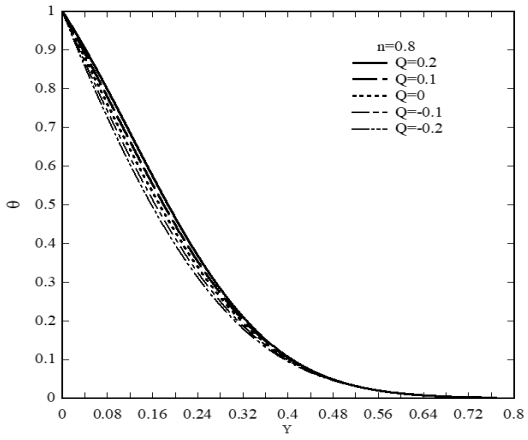

Fig. 3. Temperature profiles for α=0.1, Ri=10, Pr=20, n=0.8, and different Q.

Fig. 4 and *Fig. 5* illustrate the effect of the Prandtl number on heat transfer and hydrodynamic characteristics through the distributions of the local Nusselt number and skin friction coefficient for Ri=50, α=0.15, and Q=0.1, considering a power-law non-Newtonian fluid with different viscosity indices. The results indicate that increasing the Prandtl number leads to a reduction in the skin friction coefficient. This behavior can be attributed to the enhanced sensitivity of the fluid to buoyancy forces as the Prandtl number increases, which induces more pronounced variations in the near-wall velocity gradient (*Fig. 6*). Consequently, the wall shear stress is altered, resulting in noticeable changes in the skin friction coefficient.

On the other hand, an increase in the Prandtl number causes a reduction in the thermal boundary layer thickness. Since the wall temperature is kept constant, the temperature gradient at the wall becomes steeper (*Fig. 7*), which directly enhances the local Nusselt number. The influence of the power-law viscosity index is also evident in *Fig. 4* and *Fig. 5*. Near the leading edge of the plate, the dilatant fluid (n=1) exhibits a higher local Nusselt number compared to the Newtonian (n=1) and pseudoplastic (n=0) fluids. However, as the flow develops downstream, the local Nusselt number gradually decreases and reaches a minimum value. In contrast, the opposite trend is observed for the skin friction coefficient. The dilatant fluid shows a lower skin friction coefficient near the leading edge compared to the Newtonian and pseudoplastic fluids, whereas its value increases progressively in the downstream region. It should be noted that for the wavy surface, forced convection dominates the heat transfer mechanism in the vicinity of the leading edge, while natural convection becomes the prevailing mode further downstream. The acceleration of the fluid in the downstream region

significantly modifies the wall shear stress distribution, thereby affecting both the skin friction coefficient and the heat transfer rate.

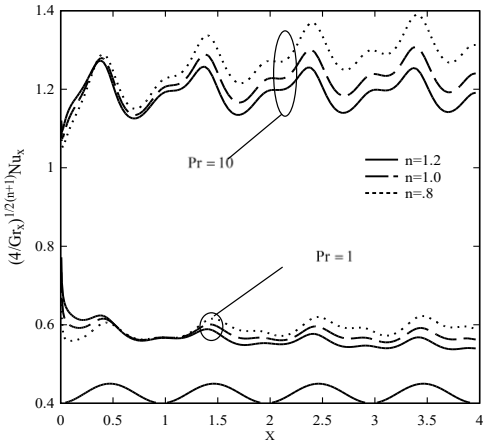

Fig. 4. Axial distribution of the local Nusselt number $\left(4/Gr_{\bar{x}}\right)^{1/2(n+1)} Nu_{\bar{x}}$ for Q=0.1, α=0.15, Ri=50, Pr=1.10, and different power-law indices.

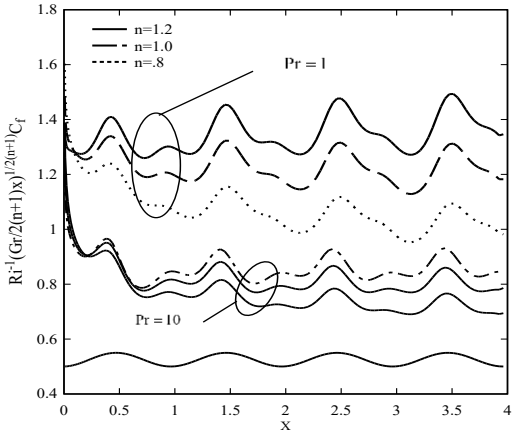

Fig. 5. Axial distribution of the skin friction coefficient $Ri^{-1}\left(\frac{Gr}{2(n+1)x}\right)^{1/2(n+1)} C_f$ for Q=0.1, α=0.15, Ri=50, Pr=1.10, and different power-law indices.

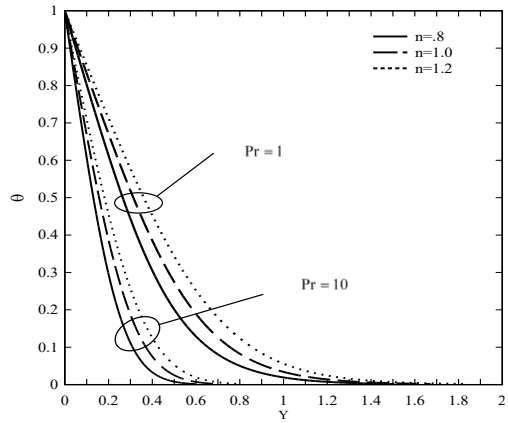

Fig. 6. Temperature profiles for Q=0.1, α=0.15, Ri=50, Pr=1-10, and different power-law index in $x = 0.75$.

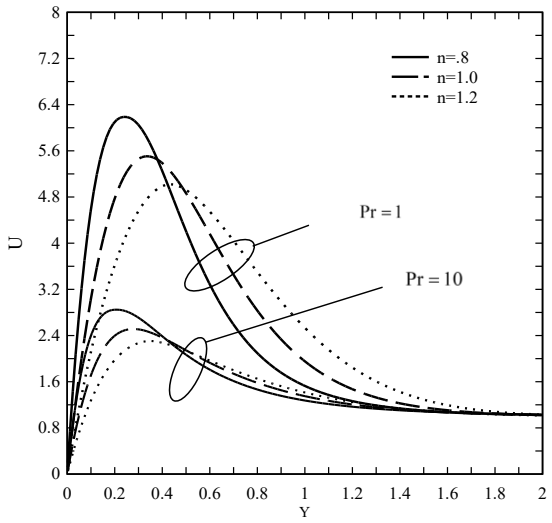

Fig. 7. Velocity profiles for Q=0.1, α=0.15, Ri=50, Pr=1-10, and different power-law index in x = 0.75.

Fig. 8 and *Fig. 9* present the axial distributions of the local and average Nusselt numbers for Q=0.1, Ri=50, Pr=10, considering different viscosity indices of the non-Newtonian fluid as well as different wave amplitudesα=0.0, 0.1, and 0.20.

The results show that, similar to free convection heat transfer investigated by Kim [1], except in the vicinity of the leading edge, the ratio of the wave amplitude to the local Nusselt number and the skin friction coefficient is approximately half of the wave amplitude of the wavy surface. Moreover, increasing the wave amplitude leads to a reduction in both the local Nusselt number and the skin friction coefficient.

The average Nusselt number also exhibits a periodic behavior; however, its oscillation amplitude is smaller than that of the local Nusselt number. In addition, the average Nusselt number for the wavy surface is higher than that of the flat surface. This enhancement can be attributed to the larger effective heat transfer area provided by the wavy geometry compared to the flat plate, which results in an overall increase in the heat transfer rate. In other words, increasing the wave amplitude enhances the average Nusselt number, indicating improved overall heat transfer performance for the wavy surface.

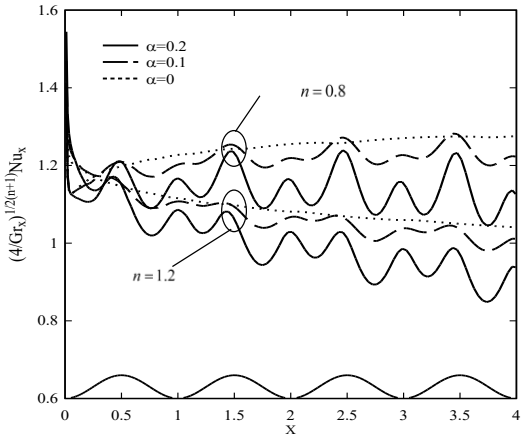

Fig. 8. Axial distribution of the local Nusselt number $\left(4/\mathrm{Gr}_{\bar{x}}\right)^{1/2(n+1)}\mathrm{Nu}_{\bar{x}}$ for Q=0.1, Ri=50, Pr=10, and different power-law indices.

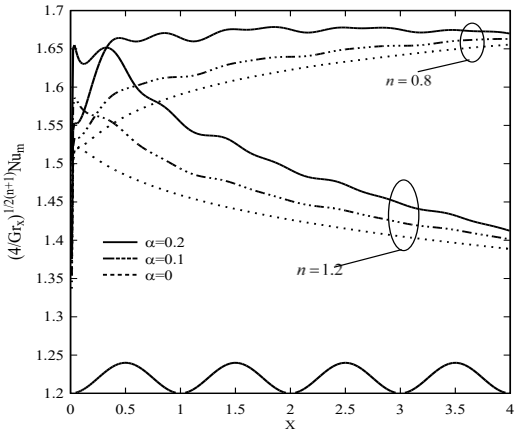

Fig. 9. Axial distribution of the average Nusselt number for Q=0.1, Ri=50, Pr=10, and different power-law indices.

5 | Conclusion

In this study, mixed convection heat transfer of a non-Newtonian power-law fluid with internal heat generation or absorption over a vertical wavy surface was numerically investigated. To simplify the geometry, an appropriate coordinate transformation was employed to convert the wavy surface into an equivalent flat surface, and the governing equations were solved using the finite difference numerical method. The effects of key physical and geometrical parameters, including the heat generation or absorption parameter, the generalized Prandtl number, the wave amplitude, and the power-law viscosity index of the non-Newtonian fluid, were analyzed through variations of the local and average Nusselt numbers. The main findings of the present study can be summarized as follows:

I. For mixed convection over wavy surfaces, forced convection is the dominant heat transfer mechanism in the vicinity of the leading edge, whereas natural convection becomes dominant in the downstream region.

II. The rate of heat transfer from the heated surface decreases with an increase in the heat generation parameter.

III. Increasing the generalized Prandtl number leads to an enhancement of both the local and average Nusselt numbers, while the skin friction coefficient decreases.

IV. The overall heat transfer rate for wavy surfaces is higher than that for a flat surface, mainly due to the larger effective heat transfer area provided by the wavy geometry.

Conflict of Interest

The authors declare that there are no conflicts of interest regarding the publication of this paper.

Data Availability

The datasets generated and/or analyzed during the current study are included in this article.

Funding

This study was carried out without any specific funding from public, commercial, or non-profit organizations.

References

[1] Kim, E. (1997). Natural convection along a wavy vertical plate to non-newtonian fluids. *International journal of heat and mass transfer, 40*(13), 3069–3078. https://doi.org/10.1016/S0017-9310(96)00357-2

[2] Yang, Y. T., Cha, O., Chen, K., & Lin, M. T. (1996). Natural convection of non-newtonian fluids along a wavy vertical plate including the magnetic field effect. *International journal of heat and mass transfer*, *39*(13), 2831–2842. https://doi.org/10.1016/0017-9310(95)00354-1

[3] Wang, C. C., & Chen, C. K. (2005). Mixed convection boundary layer flow on inclined wavy plates including the magnetic field effect. *International journal of thermal sciences*, *44*(6), 577–586. https://doi.org/10.1016/j.ijthermalsci.2005.02.001

[4] Wang, C. C., & Chen, C. K. (2002). Mixed convection boundary layer flow of non-Newtonian fluids along vertical wavy plates. *International journal of heat and fluid flow*, *23*(6), 831–839. https://doi.org/10.1016/S0142-727X(02)00145-5

[5] Jang, J. H., & Yan, W. M. (2004). Mixed convection heat and mass transfer along a vertical wavy surface. *International journal of heat and mass transfer*, *47*(3), 419–428. https://doi.org/10.1016/j.ijheatmasstransfer.2003.07.020

[6] Molla, M. M., & Hossain, M. A. (2007). Radiation effect on mixed convection laminar flow along a vertical wavy surface. *International journal of thermal sciences*, *46*(9), 926–935. https://doi.org/10.1016/j.ijthermalsci.2006.10.010

[7] Hady, F. M., Mohamed, R. A., & Mahdy, A. (2006). MHD free convection flow along a vertical wavy surface with heat generation or absorption effect. *International communications in heat and mass transfer*, *33*(10), 1253–1263. https://doi.org/10.1016/j.icheatmasstransfer.2006.06.007

[8] Tashtoush, B., & Al Odat, M. (2004). Magnetic field effect on heat and fluid flow over a wavy surface with a variable heat flux. *Journal of magnetism and magnetic materials*, *268*(3), 357–363. https://doi.org/10.1016/S0304-8853(03)00547-X

[9] Elgazery, N. S., & Abd Elazem, N. Y. (2009). The effects of variable properties on MHD unsteady natural convection heat and mass transfer over a vertical wavy surface. *Meccanica*, *44*(5), 573–586. https://doi.org/10.1007/s11012-009-9197-z%0A%0A

[10] Parveen, N., & Alim, M. A. (2011). Effect of temperature-dependent variable viscosity on magnetohydrodynamic natural convection flow along a vertical wavy surface. *International scholarly research notices*, *2011*(1), 505673. https://doi.org/10.5402/2011/505673

[11] Nath, S., & Parveen, N. (2014). Effects of viscous dissipation and heat generation on magneto hydrodynamics natural convection flow along a vertical wavy surface. *American journal of applied mathematics*, *2*(6), 197–203. 10.11648/j.ajam.20140206.11

[12] Islam, T., & Parveen, N. (2017). Natural convection flow along a vertical wavy surface with the effect of viscous dissipation and magnetic field in presence of Joule heating. *Procedia engineering*, *194*, 457–462. https://doi.org/10.1016/j.proeng.2017.08.171

[13] Amin, M. N. (2018). Numerical study on free convection flow with joule heating, heat generation and viscous dissipation along a vertical wavy surface. *Bangladesh university of engineering and technology*. http://lib.buet.ac.bd:8080/xmlui/handle/123456789/5034

[14] Mirzaei Nejad, M., Javaherdeh, K., & Moslemi, M. (2015). MHD mixed convection flow of power law non-Newtonian fluids over an isothermal vertical wavy plate. *Journal of magnetism and magnetic materials*, *389*, 66–72. https://doi.org/10.1016/j.jmmm.2015.04.043

[15] Vajravelu, K., & Hadjinicolaou, A. (1993). Heat transfer in a viscous fluid over a stretching sheet with viscous dissipation and internal heat generation. *International communications in heat and mass transfer*, *20*(3), 417–430. https://doi.org/10.1016/0735-1933(93)90026-R

[16] Yao, L. S. (1988). A note on Prandtl's tranposition theorem. *Journal of heat transfer (Transcations of the asme American society of mechanical engineers), series c;(United States)*, *110*(2). https://doi.org/10.1115/1.3250515

[17] Ghosh Moulic, S., & Yao, L. S. (1989). Mixed convection along a wavy surface. *ASME journal of heat and mass transfer*, *11*(4), 974–979. https://doi.org/10.1115/1.3250813